Remote sensing provides new insights on phytoplankton biomass dynamics and black pearl oyster life-history traits in a Pacific Ocean deep atoll

Sébastien Lefebvre, Martine Rodier, Nathanaël Sangare, Serge Andréfouët, Charles Verpoorter

Marine Pollution Bulletin 181 (2022) 113863

Contents lists available at ScienceDirect

Marine Pollution Bulletin

journal homepage: www.elsevier.com/locate/marpolbul

Remote sensing provides new insights on phytoplankton biomass dynamics and black pearl oyster life-history traits in a Pacific Ocean deep atoll

Sébastien Lefebvre [a,*], Charles Verpoorter [a], Martine Rodier [b], Nathanaël Sangare [c], Serge Andréfouët [d]

[a] UMR 8187 LOG (Laboratory of Oceanology and Geosciences), Univ Lille, ULCO, CNRS, IRD, station marine de Wimereux, 59000 Lille, France
[b] UMR 7294 MIO (Institut de Recherche pour le Développement, Aix Marseille Univ., Université de Toulon, Centre National Recherche Scientifique/INSU), 13288 Marseille, France
[c] Ifremer, UMR Ecosystèmes Insulaires Océaniens, UPF, ILM, IRD, Taravao, F-98719, Tahiti, French Polynesia
[d] UMR 9220 ENTROPIE (Institut de Recherche pour le Développement, Université de la Réunion, Centre National Recherche Scientifique, Ifremer, Université de la Nouvelle-Calédonie) Noumea, New Caledonia

ARTICLE INFO

Keywords:
Landsat-8, time series
Plankton
Aquaculture
DEB model
Pinctada margaritifera

ABSTRACT

Thus far, no long-term *in situ* observation of planktonic biomass have been undertaken to optimize the black-lip pearl oyster aquaculture in the remote Tuamotu atolls. The feasibility of using data from the OLI sensor onboard Landsat-8 satellite to determine chlorophyll *a* concentrations (*Chla*) in a deep atoll, Ahe, was then assessed over the 2013–2021 period using 153 images. Validations with *in situ* observations were satisfactory, while seasonal and spatial patterns in *Chla* were evidenced within the lagoon. Then, a bioenergetic modelling exercise was undertaken to estimate oyster life-history traits when exposed to the retrieved *Chla*. The outputs provide spatio-temporal variations in pelagic larval duration (11.1 to 30.6 days), time to reach commercial size (18.8 to 45.3 months) and reproductive outputs (0.5 to 1.7 event year^{-1}). This first study shows the potential of using remote sensing to monitor the trophic status of deep pearl farming lagoons and help aquaculture management.

1. Introduction

Atolls are ring-shaped coral reefs enclosing a lagoon, located principally throughout the Indo-Pacific under tropical or sub-tropical climates (Kinsey and Hopley, 1991). Atoll lagoons are highly productive ecosystems compared to the ultra-oligotrophic surrounding waters and often support significant ecosystem services such as tourism and aquaculture (Andréfouët et al., 2012b). In French Polynesia and in the Tuamotu-Gambier archipelago in particular, black pearl aquaculture is based on the culture of one suspension-feeder bivalve, the black lip pearl oyster, *Pinctada margaritifera*, and this activity is the second source of incomes for French Polynesia territory. However, fluctuations in the production of pearls over the last 20 years have originated from environmental variations that are difficult to evaluate in real-time in these remote atoll ecosystems (Andréfouët et al., 2022b).

Pearl oysters are able to process seston particles efficiently as small as 3 µm (Pouvreau et al., 1999), so that, in atoll lagoons, nanophytoplankton and mixotrophic and heterotrophic cells, form the bulk of their diet (Loret et al., 2000). However, most of the autotrophic biomass (*ca.* 80 %) is formed by picophytoplankton (<2 µm, cyanobacteria and picoeukaryotes), too small particles to be consumed efficiently by oysters (Fournier et al., 2012a). In fact, picophytoplankton is consumed by the mixotrophic and heterotrophic cells which act as trophic mediators between picophytoplankton and oysters (Loret et al., 2000). Thus, even if the plankton biomass is mainly composed of picophytoplankton, chlorophyll *a* concentrations (*Chla*) were confirmed to be an appropriate proxy of food availability for pearl oysters (Sangare et al., 2020). Life-history traits of the pearl oyster such as growth, reproduction and recruitment (including spat collection for the pearl oyster farms) depend strongly on the food availability and water temperature (Fournier et al., 2012b; Thomas et al., 2012; Sangare et al., 2020) which differ in gradients between as well as within atoll lagoons. As a result, both juvenile and adult growth differences are reported between atoll lagoons (Pouvreau and Prasil, 2001) and within an atoll lagoon (Sangare et al., 2020). Adult reproduction also varies at the seasonal scale (Fournier et al., 2012b). Finally, bivalve larvae biomass and spat collection vary in space and time within an atoll (Thomas et al., 2012). Hence, it is considered that a sustainable black pearl production

* Corresponding author.
E-mail address: sebastien.lefebvre@univ-lille.fr (S. Lefebvre).

https://doi.org/10.1016/j.marpolbul.2022.113863
Received 15 February 2022; Received in revised form 8 June 2022; Accepted 14 June 2022
Available online 7 July 2022

industry requires a good knowledge of *Chla* and water temperature to take appropriate management decisions.

Pearl culture has been established in many French Polynesia atolls, but not all of them have been studied in detail. Oceanographic campaigns were performed in late 90s to sample 10 atolls to study their trophic status once (*i.e.*, one or two days of measurements) during two seasons (Dufour and Harmelin-Vivien, 1997). The atoll geomorphology (depth, openness to the ocean) and exposure to prevailing waves and winds control water residence time which greatly influences the lagoon trophic status and food web organization. As the geomorphology may differ from one atoll to another, this leads to a wide range of lagoon ecological functioning (Pagès et al., 2001; Dufour et al., 2001). *Chla* ranges typically between 0.18 and 1.24 $\mu g.L^{-1}$ between atoll lagoons (Pagès et al., 2001). As Tuamotu-Gambier atolls are spread over large areas (approximately 4840 km^2), these ecosystems are difficult to survey on a long-term basis and studies of spatio-temporal variability within atolls are scarce. Historically, the atolls of Takapoto (and to a lesser extent Tikehau) in the 90s and Ahe (and Takaroa) since 2007 have been the most studied, especially in the planktonic compartment. Delesalle et al. (2001) reported spatial heterogeneity in phytoplankton biomass during several seasons in Takapoto atoll and Charpy (1996) described the temporal variability on a monthly scale in Takapoto atoll. More recently, the spatial and temporal variabilities were characterized in Ahe atoll (Thomas et al., 2010; Lefebvre et al., 2012; Sangare et al., 2020; Rodier et al., 2021). The spatio-temporal variations in *Chla* are driven by the water residence time which varies daily due to differences in swell, wind and tide conditions (Andréfouët et al., 2001), but also varies spatially within atoll lagoon depending on water circulation, and wind conditions (Thomas et al., 2010; Dumas et al., 2012; Fournier et al., 2012b). *Chla* is also affected by wet and dry seasons and water temperature (Lefebvre et al., 2012; Thomas et al., 2012). However, quantifying the extent of these spatio-temporal variations in phytoplankton biomass and their effects on pearl oyster performances are not possible without long-term survey of the phytoplankton compartment, but also without a relatively high frequency sampling as the conditions may vary quickly, in a matter of days, according to the environmental conditions.

Satellite remote sensing has been proven to be a valuable method for assessing water quality and for supporting aquaculture management (Palmer et al., 2020). The choice of a remote sensing method is the result of trade-offs between spectral, spatial, temporal resolution of sensors depending on the question raised (McCarthy et al., 2017). Among available sensors passing over the study area, two optical satellites are of interest for oligotrophic clear waters in atoll lagoons in an aquaculture context, namely the OLI (Operational Land Imager) sensor onboard Landsat-8 satellite (L8) allowing acquisitions at high spatial resolution (30 m/pixel) every 16 days and the OLCI (Ocean and Land Colour Instrument) sensor onboard Sentinel-3A/B satellite (S3A/B) allowing the acquisition of scenes at medium spatial resolution (300 m/pixel) every ~2 days at Tuamotu latitudes. Due to their spectral and radiometric resolutions OLI and OLCI are perfectly suitable to measure *Chla* from the reflectance of water. The high spatial resolution of L8 allows for better mapping of spatial variations within small structures such as lakes (*e.g.* Ruiz-Verdu et al., 2016) and hence potentially atoll lagoons as well. Although L8 images have been used in many studies to quantify *Chla* such as in Lake Titicaca (Ruiz-Verdu et al., 2016) or coastal waters of the US Virgin Islands (Kerrigan and Ali, 2020), none of them have focused on Pacific Ocean atoll lagoons yet to our knowledge.

Based on a quantitative evaluation between remote sensing reflectance (R_{rs}) from Landsat-8 and *in situ* data, Wei et al. (2018) confirmed that L8 measurements are appropriate for coral reef application but pointed out that in these optically clear-water ecosystems, bottom reflectance has to be considered when studying the properties of the water column (Boss and Zaneveld, 2003). Two solutions emerge: either the removal of the bottom contribution to the signal measured by the satellite but this remains challenging (McCarthy et al., 2017) or more simply the elimination of the problematic shallow areas by masking them. A depth of *circa* 20 m has been evidenced by several authors to be the threshold for the detection of the bottom reflectance in such waters (*e.g.* Kutser et al., 2020). However, this depends on the type of bottom-albedo as bright substrates, such as coral sand and mud will influence more strongly the total signal with an enhanced contribution to the upwelling signal compared to coral, algae or bare rock substrates (Maritorena et al., 1994; Ackleson et al., 2018). This means that only atolls with a significant deep lagoon surface area such as Ahe (average depth of 41 m Andréfouët et al., 2020) are worth investigating to check if *Chla* can be accurately remotely sensed.

The use of satellite remote sensing for marine aquaculture applications has been fruitful for site selection (McCarthy et al., 2017). To this end, remotely sensed *Chla* and water temperature data were efficiently coupled with individual bioenergetic models to produce spatio-temporal growth trajectories of cultured bivalves (*e.g.* Brigolin et al., 2017). In some cases, Dynamic Energy Budget models (or DEB; Thomas et al., 2011b, Palmer et al., 2020) were used. The DEB theory is a generic approach that assumes common metabolic organization and energy allocation rules between species whatever their life stages are, *via* a set of parameters, some of which can be species-specific (Sousa et al., 2008). DEB models are useful to understand the acquisition of energy (proportional to the surface area of the organism) and the allocation of this energy towards growth and its maintenance on the one hand, and reproduction and the acquisition of maturity and its maintenance on the other hand. A DEB model has recently been developed for all *Pinctada margaritifera* life stages (Sangare et al., 2020). This model uses water temperature and *Chla* (as a proxy for food availability) as forcing variables. This development is particularly interesting for modelling both the larval processes (development and recruitment) and the growth of juveniles and reproduction of adults, three life stages that are all critical for the pearl oyster aquaculture industry (Andréfouët et al., 2012b; Sangare et al., 2020).

Data on the spatio-temporal dynamics of phytoplankton in Tuamotu atoll lagoons are patchy and hinder a better understanding of their ecological functioning but also of their aquaculture productivity. The aim of the present study was therefore to assess the feasibility and advantages of a remote sensing approach coupled to a bioenergetic modelling approach to improve knowledge of deep atoll lagoons functioning and discuss the implications for pearl oyster aquaculture. The deep lagoon of Ahe atoll was used as a case study. Firstly, seven years and half of reflectance image archives of the OLI (Operational Land Imager) sensor onboard Landsat-8 satellite (L8) were used at the scale of Ahe lagoon in order to produce spatial and temporal trends in phytoplankton biomass as represented by chlorophyll *a* concentrations ($Chla^a$). An *in situ* survey allowed to assess some observed temporal and spatial patterns using the temporally closest observations from a Landsat overpass. A particular attention was paid to the effects of bottom reflectance through a more detailed study of the effects of bathymetry on the computed chlorophyll *a* values. The L8-OLI remotely sensed *Chla* products were also compared with remotely sensed Ocean-Colour data from the European Space Agency (ESA) Climate Change Initiative project (OC-CCI) V5.0 products at 1 km and one day resolution. Secondly, spatio-temporal fluctuations in trophic resource (*Chla*) and water temperature were used to force a DEB model to predict how several life-history traits of the pearl oyster (adult growth and reproduction, pelagic larval duration) will vary depending on Ahe atoll environmental conditions. MODIS-Aqua sea surface temperature (SST) products were used to provide water temperature for DEB modelling.

2. Material and methods

2.1. Study site

Ahe Atoll (14.5° S, 146.3° W) is located in the northwestern part of the French Polynesia Tuamotu Archipelago, 500 km northeast of the

island of Tahiti in the Pacific Ocean. The dimensions of the atoll are 23.5 km long and a maximum of 12.2 km wide (Fig. 1). The bathymetry of the lagoon was charted completely using a mono-beam depth sounder as described in Andréfouët et al. (2020). The 145 km^2 lagoon has an average depth of 40.6 m and a maximum depth of 71 m. The shallowest parts (<30 m) are restricted to the edges of the reef rim, lagoon pinnacles and also includes the south-western part of the lagoon. In total, this represents *ca* 21 % of the total surface (~30 km^2). The lagoon is connected to the surrounding ocean by a deep pass in the west and by numerous shallow channels (or *hoa*) in the south and west but the water exchange with the ocean is considered moderate due to a low exposure to oceanic waves (Andréfouët et al., 2012a). Therefore, Ahe lagoon is defined as hydrodynamically semi-enclosed. The climate is humid tropical with a rainy season ranging from November to April. The water temperature in the lagoon varies typically between 26 and 30 °C (Thomas et al., 2010; Sangare et al., 2020). Ahe has been a pilot site for the pearl farming research program since 2007 (Andréfouët et al., 2012b) as it hosts significant pearl farming activity, although it has declined in the past years.

2.2. Ocean-colour remotely sensed data

Three kinds of data sets were used from satellite sensors. Near-surface chlorophyll *a* concentrations (*Chla*) were retrieved from Landsat-8 Operational Land Imager using a chlorophyll algorithm after correcting for atmospheric effects. The two other datasets were retrieved directly from spatial agencies as final products without specific processing: *Chla* from Ocean-Colour data initiative of the European Space Agency (ESA) and Sea-Surface Temperature from MODIS Aqua of the National Aeronautics and Space Administration (NASA).

2.2.1. Chlorophyll a concentrations processed from Landsat-8 Operational Land Imager

The present study is based on the Level-1 daily Landsat-8 (L8) data of the multispectral OLI (Operational Land Imager) sensor. Landsat-8 OLI sensor consists of nine spectral bands (band 1 - coastal aerosol; band 2 - blue, band 3- green, band 4 - red; band 5 - Near Infrared NIR; band 6 – SWIR1; band 7 - SWIR2; band 8 - panchromatic; and band 9 – cirrus) with a 30-m resolution. Data are available on USGS gateway (https://earthexplorer.usgs.gov/) and were acquired from 05/26/2013 to 04/14/2021. The satellite collects images of the Ahe atoll with a 16-day repeat cycle, referenced to the Worldwide Reference System-2. Approximate scene size is 170 km north-south by 183 km east-west. Using USGS platform visualization tool, a rapid and easy identification of suitable scenes for time-series pixel level analysis was performed based on cloud cover and wind effect on the ocean and lagoon surface. Only images representing a sufficient amount of valid pixel over Ahe were kept and analyzed, which represented a total of 153 scenes (and therefore days).

Retrieval of remote sensing reflectance (R_{rs}) products from satellite imagery requires atmospheric correction (AC). In attempting to assess the *Chla* in lagoon, elimination of atmospheric effects and water surface scattering from the upward radiance is an essential step in order to observe backscattered photons which contain only information about the subsurface condition (Gordon, 1978). In the present study, a generic processor called ACOLITE (Atmospheric COrrections of satellite, V.20210802.0; Vanhellemont and Ruddick, 2018; Vanhellemont, 2019) was used for atmospheric correction and pre-processing of atoll water prior to deriving near-surface chlorophyll *a* concentrations (*Chla*) in Ahe atoll. ACOLITE is based on radiative transfer theory. This tool supports high spatial resolution products such as L8-OLI and it is able to minimize sun-glint effects. Among the AC algorithms, Wei et al. (2018) provide a quantitative evaluation of Landsat-8 R_{rs} and concluded that the ACOLITE AC method is suitable for water masses such as found on coral reefs.

In this study, the ACOLITE/SWIR approach was used for aerosol determination (Vanhellemont and Ruddick, 2018) considering the assumption of zero water-leaving radiance (ρ_w) is valid (also known as "black pixels"). The ACOLITE AC assumes that due to exceedingly high

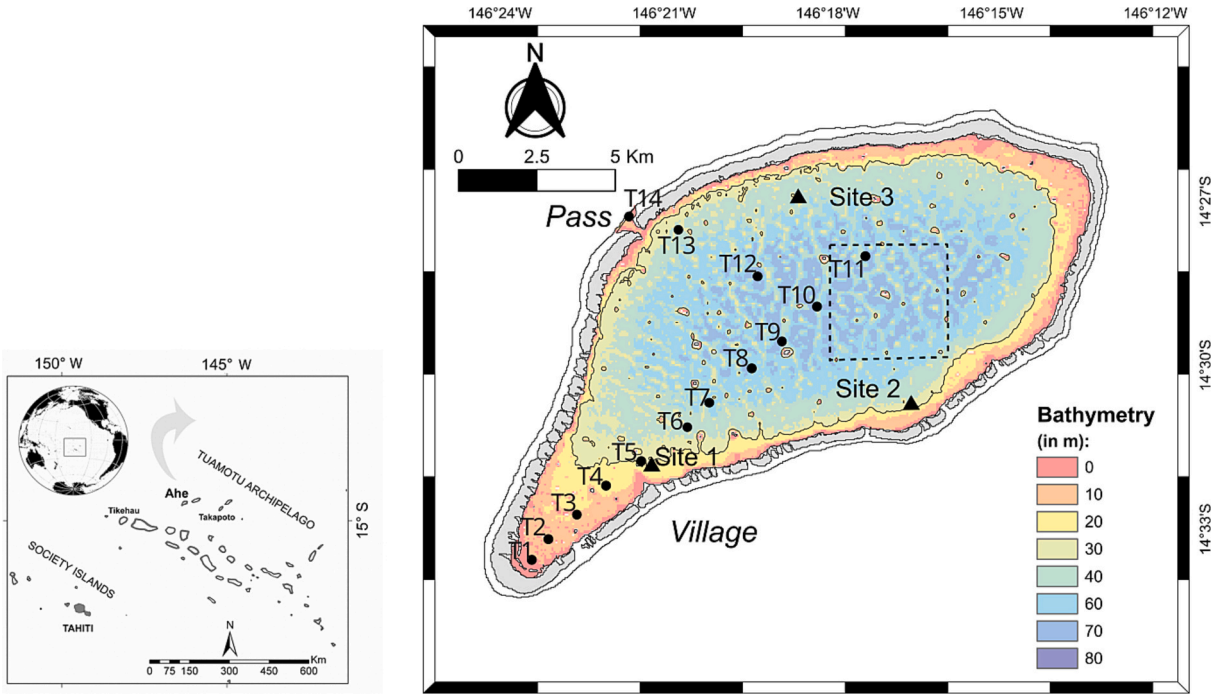

Fig. 1. Map of Ahe atoll, its location in Tuamotu Archipelago and lagoon bathymetry. Location of survey sites where chlorophyll *a* concentrations (*Chla*) were estimated using *in situ* sampling and remotely sensed data. Black triangle: temporal survey; Points: spatial survey (the transect sites are consecutively numbered from T1 in the south-west corner to T14 in the pass, T11 being the most north-western site); Squared area: temporal survey using ESA Ocean colour CCI *Chla* products V5 at 1 km/pixel and NASA Ocean Colour MODIS SST products at 4 km/pixel. (For interpretation of the references to colour in this figure legend, the reader is referred to the web version of this article.)

pure-water absorption in the shortwave infrared (SWIR) of the spectral domain at 1.6 and 2.2 μm the signal remaining in these bands after Rayleigh correction is induced by aerosol scattering. By default, ACOLITE was set based on the Dark Spectrum Fitting (DSF) method (Vanhellemont, 2019) which consists in measuring the radiance of the darkest pixel in order to estimate the impact of atmospheric effects by estimating water vapor, clouds and aerosols on a per-pixel basis. A cirrus cloud masking procedure, and a sun glint contamination correction were performed in ACOLITE using default parameters. In practice, to remove first the non-water pixels (*e.g.* clouds, wave breaking, or land pixels), and to correct glint effects from water pixels, a threshold (<0.05) on the reflectance in the 1.6 μm SWIR band was performed. The sun glint correction was based on the Harmel et al. (2018) procedure for which an estimate of the glint reflectance was made in a range of SWIR bands and extrapolated to the shorter wavelength channels (VNIR) using a model reflectance shape. Negative pixels were also masked.

Near-surface chlorophyll *a* concentrations (*Chla* in mg m^{-3} or equivalently in μg L^{-1}) were calculated using the chlorophyll *a*lgorithm currently used by NASA (see https://oceancolor.gsfc.nasa.gov/atbd/chlor_a/). This algorithm consists in merging the standard OCx band ratio algorithm (O'Reilly et al., 1998), which is called OC3 for Landsat OLI sensor, and the colour index (CI) developed by Hu et al. (2012). The NASA operational OC3 algorithm is a four-order polynomial relationship derived from R_{rs} and *in situ* measurements of *Chla*, and a three order-band algorithm using the maximum band ratio of blue bands (443/482 nm) and green band (561 nm). Global validation exercise using large *in situ* NASA bio-Optical Marine Algorithm Dataset (NOMAD v2, https://seabass.gsfc.nasa.gov/wiki/NOMAD) has shown a better performance of CI compared to the OC3 algorithm with a significant reduction of the uncertainties and biases associated with residual glint, stray light, AC errors, and white or spectrally-linear bias error in R_{rs} for $Chla \leq 0.15\ \mu g\ L^{-1}$ (oligotrophic waters). With the intention to ensure a smooth transition between water types, the used algorithm follows the NASA procedure which diverges slightly from Hu et al. (2012). Indeed, the CI algorithm is restricted to relatively clear waters at $Chla \leq 0.15\ \mu g\ L^{-1}$ while the OC3 is restricted at higher chlorophyll concentration waters ($Chla > 0.20\ \mu g\ L^{-1}$). In between these values ($0.15\ \mu g\ L^{-1} < Chla \leq 0.20\ \mu g\ L^{-1}$), the CI and OC3 algorithms were blended using a weighted approach (see Hu et al., 2012 for further details). We named this switching algorithm the OC3CI algorithm. To our knowledge, the OC3CI algorithm has never been applied to map *Chla* in atoll lagoon waters. As *Chla* typically ranged from 0.18 to 1.24 μg L^{-1}, OC3CI algorithm is particularly appropriate to retrieve near-surface chlorophyll *a* concentrations in these waters.

2.2.2. ESA OC-CCI chlorophyll a concentrations (Chla) and MODIS-Aqua Sea-Surface Temperature (SST) products

Two standard level 3 products were also handled for comparison with our L8 images processing.

First, remotely sensed Ocean-Colour data from the European Space Agency (ESA) Climate Change Initiative project (OC-CCI) V5.0 were used for establishing comparison with *Chla* obtained from L8-OLI level 1 products. The OC-CCI product merges and corrects the biases of data from four independent Ocean Colour sensors (*i.e.* SeaWifS, MODIS, MERIS, and VIIRS) and related algorithms and atmospheric corrections (http://www.esa-oceancolour-cci.org). The level 3 mapped *Chla* was retrieved at 1-km and a maximum 1-day resolution (but on average 3-days resolution) for the period ranging from January 2007 to May 2021 (last access in September 2021). This period encompassed both our L8 time-series and some historical data sets over the 2007–2009 and 2013 periods, hence before the L8 launch in 2013. A total of 1856 mean values were then retrieved of which 5 were discarded as they were atypical and isolated in time, *i.e.* close to 0, or higher than 1 μg L^{-1}. Another seven consecutive values were deleted from 01-06-2012 to 13-06-2012, because *Chla* reached a suspicious 1.1 μg $L^{-1}$to 4.6 μg L^{-1}, although we acknowledge they could be the consequence of an atypical huge phytoplankton bloom as well.

Second, MODIS-Aqua Sea-Surface Temperature (SST) products delivered from the NASA Ocean Colour website (http://oceancolor.gsfc.nasa.gov) were used in this study for monitoring seasonal changes in Ahe atoll temperature for the period 01/01/2007 to 03/22/2021 providing a comparable time series to the OC-CCI one. Level 3-SST mapped products were temporally binned into 8-day climatology and with a 4 km spatial resolution. The night-time SST observations derived from the 11-micron spectral band were computed following the long-wave infrared (LWIR) algorithm which is a modified version of the nonlinear SST algorithm of Walton et al. (1998). A total of 584 mean values were then retrieved. Pixels with depth higher than 30 m were selected, yielding only two usable lagoon pixels for MODIS-Aqua. The pixel with the lower density of pinnacles was chosen as these coral structures at sub-surface may affect the remotely sensed data. Note that we aim to use SST to assess the general trend variations across our time-series and to use representative values for DEB modelling, and not to characterize precisely the lagoon temperature throughout the lagoon as in Van Wynsberge et al. (2020),. A common bounding box was then selected for both products (146°18.42 W 14°28.2 S and 146°16.2 W 14°30.36 S) corresponding to 1 pixel for SST product and 16 pixels for OC-CCI product (Fig. 1).

2.3. Survey sites in the lagoon, in situ available data sets for match-ups and further data processings

Three survey sites (Fig. 1) with depth close to 30 m were monitored for temporal dynamics (Fig. 1, 29.9, 34.7 and 28.5 m for S1, S2 and S3 respectively) as they were shown to be environmentally contrasted (Thomas et al., 2010; Sangare et al., 2020; Rodier et al., 2021). Two of these sites (S1 & S3) were monitored over 6 months from March to August 2017 for *in vivo Chla* (daily at four 3-week periods), water temperature (daily) and pearl oyster growth (at four dates; Sangare et al., 2020). Additionally, a spatial transect (Fig. 1) was performed at two different dates (28 nov. and 2 dec. 2017) for which extracted *Chla* measurements were assessed following Rodier et al. (2021). Some other extracted *Chla* were retrieved from the table 4 of Thomas et al. (2010) for the periods May 2007, August 2007, March 2008 and August 2008 and from the table 2 of Lefebvre et al. (2012) for the periods May 2008, October 2008, February 2009, and August 2009. Two additional studies from Pagano et al. (2017) and Rodier et al. (2021) provided one value each in May 2013 and December 2017, respectively.

Remotely sensed *Chla* products from L8 OLI were averaged over a circle with a radius of 100 m (36 pixels) around each survey site. The same approach was used for the 14 sites of the transect using the closest scene available (12/31/2017), *i.e.* a month later than the sampling. Dynamics of remotely sensed *Chla* and SST were smoothed using a cubic smooth spline (function smooth.pline of the R version 4.0.3) and were interpolated every day for easing interpretation of the figures in the Results section.

The effect of bottom reflectance on remotely sensed *Chla* was assessed in two ways. First, at each date, means of *Chla* values were calculated using pixels at all depths (the whole lagoon), and for the ones up to 10 m, 20 m, 30 m, 40 m and 50 m, giving a total of six means which were normalized (centered and reduced) giving a *Z*-Score comparable between dates. Means and standard deviations of the Z-scores for all dates at the six depth intervals were then calculated. The goal was to partial out the temporal effect and to highlight a potential relationship between bathymetry and *Chla* assuming that a decreasing trend may reveal a potential effect of bottom reflectance. Second, a comparison of remotely sensed and extracted *Chla* from the spatial transect was performed against bathymetry to highlight the threshold depth at which the *Chla* signal may be positively biased.

2.4. Bioenergetic modelling

The Dynamic Energy Budget (DEB) theory (Kooijman, 2010) was used to simulate life-history traits of the black pearl oyster (*Pinctada margaritifera*) following the parametrization put forth by Sangare et al. (2020). The model has two forcing variables: 1) temperature which influences all rates through a temperature correction (TC) function and 2) food abundance as proxied by *Chla* which impacts assimilation according to a scaled Holling's type II functional response (f) using a calibrated parameter (the half saturation coefficient X_k). X_k was calibrated on the shell length dynamics of two size classes of pearl oyster at two sites (sites S1 and S3, Fig. 1) during six months in 2017 (data retrieved from Fig. 8 in Sangare et al., 2020). Fitting of the X_k value was achieved by minimizing the sum of squared residuals between predictions and observations.

Three life-history traits were of interest as they are critical for black lip pearl oyster aquaculture (Sangare et al., 2020). These are the pelagic larval duration (PLD), the juvenile/adult growth, and the adult reproduction. These three traits were simulated for the three sites along the seven and half years using linearly interpolated remotely sensed *Chla* and SST products as forcing variables.

The PLD trait was estimated from the duration between gamete release and settlement of juveniles, simulations starting at the beginning of every month along the seven and half years ($N = 85$). Settlement of juveniles occurs when the maturity threshold is reached which corresponds to a size of approximately 1.3 mm. Second, the growth trait was estimated as the time needed for recently settled juveniles to reach the grafting size (9 cm shell length). Juveniles were seeded at the start of every month, but as the food abundance differed between the sites, the total number of simulated periods by sites was different ($N = 58$ for S1, $N = 52$ for S2, $N = 39$ for S3). Third, the reproduction trait was the cumulative daily reproductive effort and potential spawning events for a 13 cm-shell length adult, a size in the upper range of cultured individuals (Pouvreau and Prasil, 2001). Spawning occurs when the gameto-somatic index reaches 0.29, and the reproduction buffer is then emptied by 0.85. Spawning is opportunistic regardless of environmental conditions see Sangare et al. (2020) for details.

All simulations were performed under Matlab 2010b and outputs were stored on a daily step.

3. Results

3.1. Sea-surface temperature (SST)

MODIS-Aqua remotely sensed SST products at 4 km resolution were retrieved for a central lagoon pixel (Fig. 1). SST displayed seasonal variations ranging from 25.6 to 31.1 °C (mean ± sd 28.3 °C ± 1.1 °C) and typically peaked in January–February and floored in September (Fig. 2A). Some inter-annual differences occurred with concomitant differences in minima and maxima of *ca* 1.5 °C. Two years, 2008 and 2011, displayed lower maxima, *ca* 28.5 and 28 °C respectively. Performance of the satellite product was evaluated using *in situ* temperature observations monitored for six months in 2017 (Fig. 2B). A small deviation from the observations occurred but the seasonal trends were coherent and the linear relationship was significant ($Y = 1.01\ X - 0.61$, $N = 17$, adj $R^2 = 0.86$; $F = 92.32$; $P < 0.001$). The difference in temperature between the two survey sites (S1 and S3; Fig. 1) was very low (on average 0.08 °C, Fig. 2B).

3.2. Spatial distribution of remotely sensed Chla and bathymetry effect

The use of L8-OLI remotely sensed chlorophyll *a* concentrations (*Chla*) allowed to perform an analysis on the effect of bathymetry to assess a potential bottom reflectance effect (Fig. 3A). The relationship between *Z*-scores of *Chla* and bathymetry decreased sharply when shallow depths were progressively excluded and stabilized when only depths higher than 30 m were considered. A match-up exercise displayed a very good agreement between remotely sensed and *in situ Chla* (spatial transect Fig. 1) in particular for sites with a depth higher than 20 m (Fig. 3B). A high discrepancy occurred for site T2 where bathymetry was 14.6 m whereas site T12 displayed a good agreement for the same depth. These two independent analyses enable to consider that a potential effect of the bottom would be negligible for depths higher than 20 m. Hereafter, we choose a conservative 30 m threshold, which still allowed to process 70 % of the lagoon.

The spatial distribution of *Chla* from L8-OLI, for waters deeper than 30 m revealed that higher *Chla* values were found (>0.4 μg L^{-1}) in the south-western part and on the edge of the eastern as well as in the northern parts (Fig. 4). Lower *Chla* values occurred in the central zone. A plume of inflowing oceanic water through the pass contrasted with the

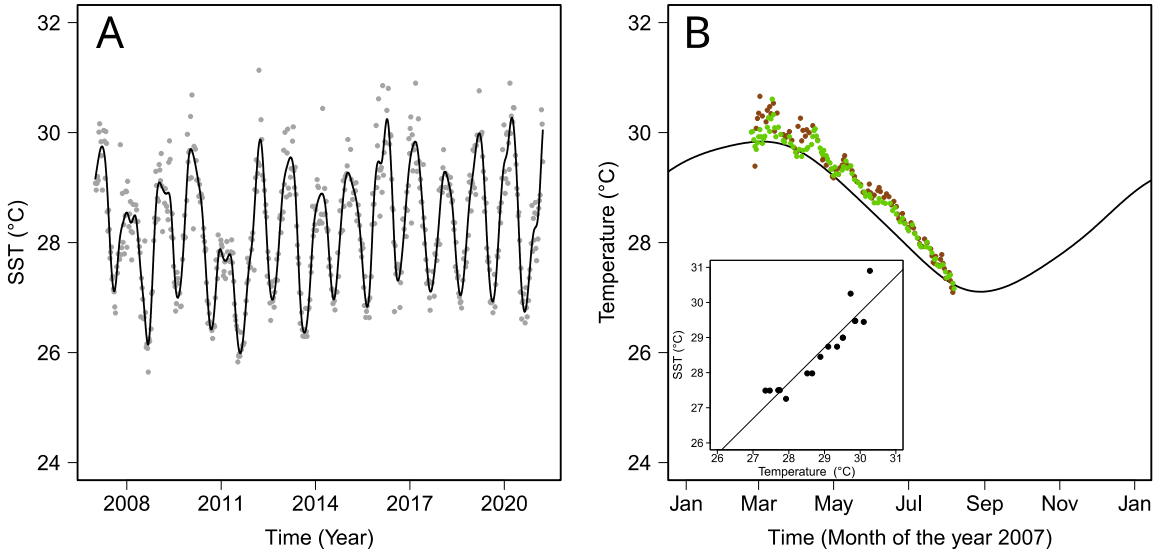

Fig. 2. A) Sea-Surface Temperature (SST) from MODIS-Aqua over 15 years, with MODIS observations (grey circles), and interpolated line (cubic smoothing spline). B) Validation of MODIS observations against two *in situ* observations temperature data sets (S1 and S3 in Fig. 1, brown and green circles respectively) for the year 2017 (data retrieved from Sangare et al., 2020). The line is the smoothed curve from panel A. The insert shows remotely sensed SST *versus in situ* temperature values. (For interpretation of the references to colour in this figure legend, the reader is referred to the web version of this article.)

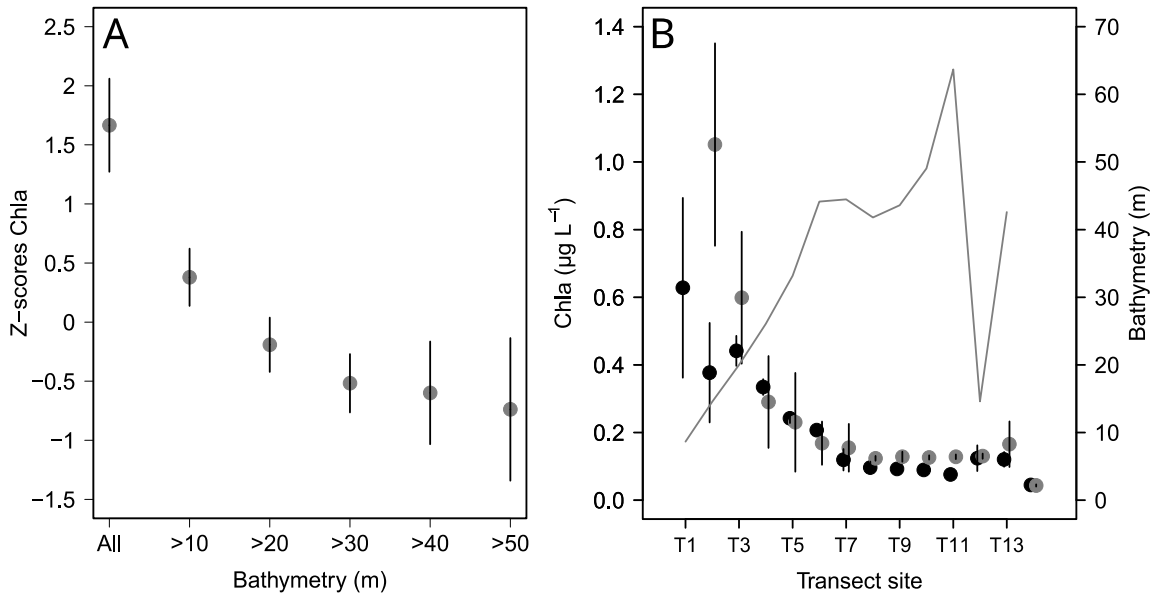

Fig. 3. Remotely sensed chlorophyll *a* concentrations (*Chla*) from L8-OLI, with A) effect of bathymetry on centered and reduced *Chla* values per date (*Z*-scores) as a function of bathymetry (see Material and methods section for details). B) Transect along 14 sites performed in 2017 (see Fig. 1 for details). Extracted *Chla* (mean and sd; black circles) and remotely sensed *Chla* (mean and sd; grey circles). The bathymetry of sites is displayed with the grey line.

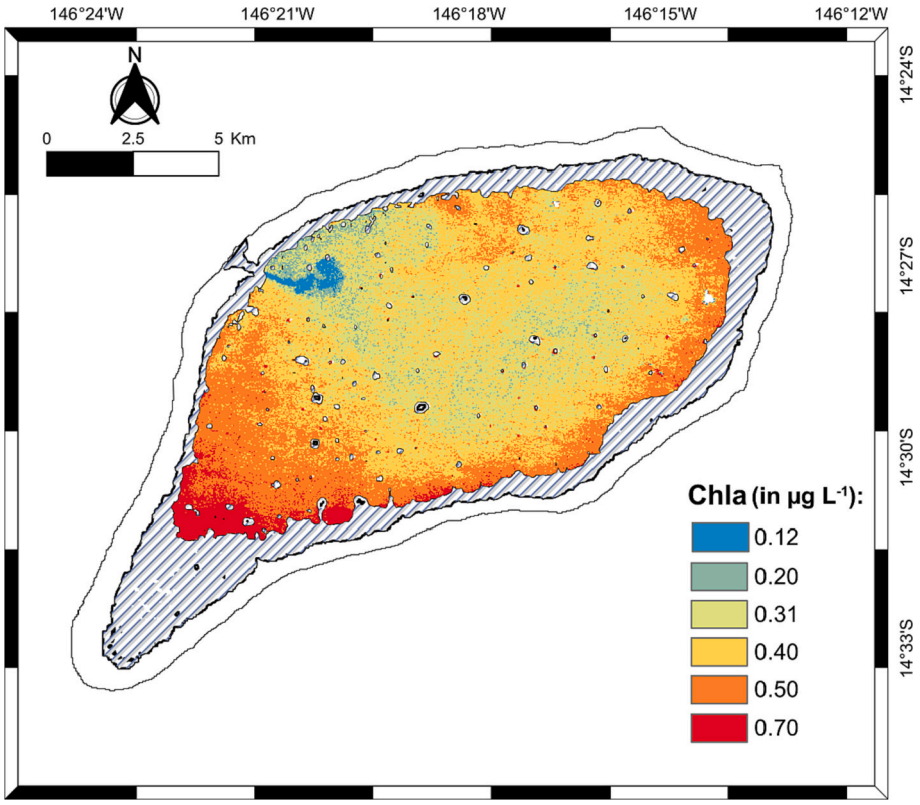

Fig. 4. Spatial distribution of chlorophyll *a* concentrations (*Chla)* from L8-OLI for waters deeper than 30 m on the date of 04/29/2019 (see Fig. 1 for bathymetry details). Note the plume of oceanic oligotrophic water (blue colour) entering the lagoon through the pass. (For interpretation of the references to colour in this figure legend, the reader is referred to the web version of this article.)

rest of the lagoon, with very low level of *Chla* values.

3.3. Temporal Chla dynamics at the three survey sites

Chla in the three temporal survey sites (Fig. 1) displayed different temporal patterns. At S1 (Fig. 5A), values ranged from 0.13 to 0.89 µg L^{-1} (mean ± sd, 0.46 ± 0.17 µg L^{-1}, $N = 93$) and exhibited clear seasonal patterns in relation to water temperature (Pearson correlation coefficient $r = 0.34$, $t = 3.4$, df = 90, $P = 0.001$). Two peaks a year could be observed. At S2 (Fig. 5B), values were slightly lower (mean ± sd, 0.31 ± 0.14 µg L^{-1}), ranging from 0.11 to 0.60 µg L^{-1}. The seasonal pattern was blurred in 2015 and 2016 but a significant correlation with

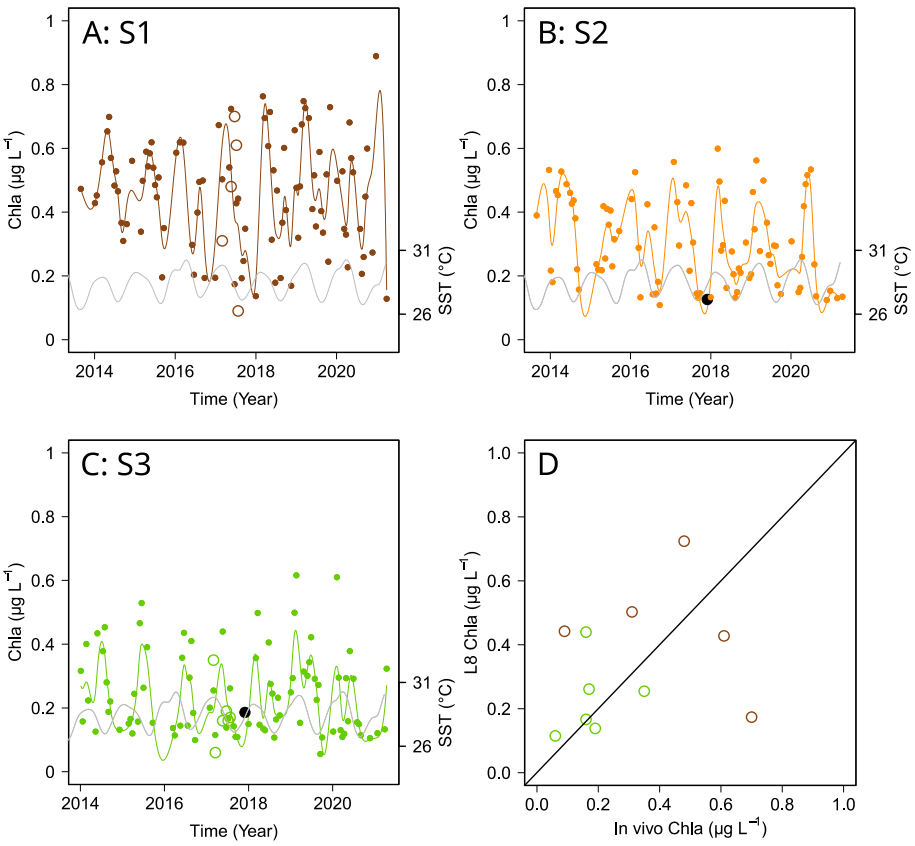

Fig. 5. A, B, C, remotely sensed chlorophyll *a* concentrations (*Chla*) from L8-OLI in the three survey sites S1 brown line, S2 orange, S3 green (filled circles are satellite observations and line is the cubic smoothing spline interpolation). Temperature dynamics from Fig. 2 were added to the three plots for ease of comparison (grey line). Open circles in A and C are *Chla* estimated by *in vivo* fluorescence measured in 2017 from Sangare et al. (2020). Black circles in B and C are *Chla* estimated after extraction from Rodier et al. (2021). D: Relationship between L8-OLI *Chla* values and *in vivo* fluorescence (match-ups only) was not significant ($P > 0.005$) ($Y = X$ identity line is shown). (For interpretation of the references to colour in this figure legend, the reader is referred to the web version of this article.)

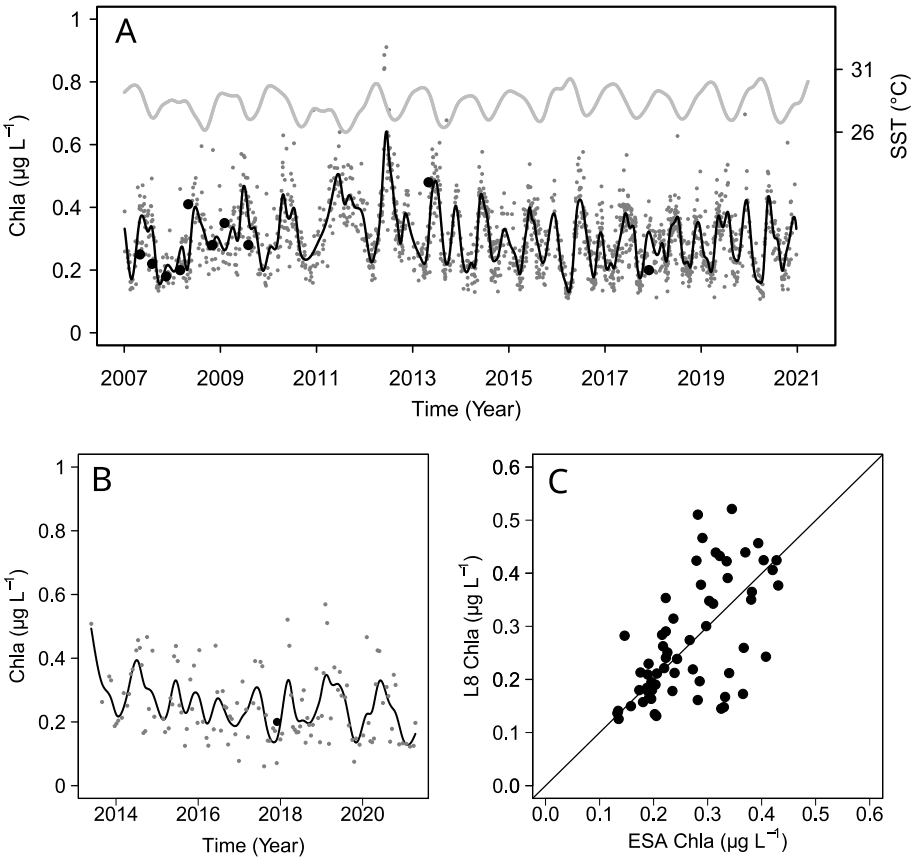

Fig. 6. Comparison of the temporal dynamics of chlorophyll *a* concentrations (*Chla*) between the two remotely sensed data sets. A) ESA Ocean Color-CCI at 1 km for a squared central area of the Ahe lagoon from 2007 to 2020 (Fig. 1). Temperature dynamics from Fig. 2 were added for ease of comparison (grey line). B) L8-OLI for the same bounding box than ESA from 2013 to 2021. C) The significant linear relationship between ESA OC-CCI product and L8-OLI *Chla* ($Y = 0.99\ X + 0.00$, $N = 63$, adj $R^2 = 0.91$; $F = 610.7$; $P < 0.001$). Grey points are remotely sensed observations, black line is the cubic smoothing spline interpolation, black points are historical *in situ* observations.

temperature was still found ($r = 0.27$, $t = 2.6$, df = 87, $P = 0.01$). Patterns in S3 (Fig. 5C) were clearly different from the two previous ones with fluctuations unrelated to temperature ($r = 0.05$, df = 82, $P = 0.63$) and lower values (mean ± sd, 0.24 ± 0.13 µg L^{-1} min-max 0.05–0.62 µg L^{-1}).

The match-up between remotely sensed *Chla* and observed values was qualitatively good as ranges of values were consistent (Fig. 5 A, B, C). However, the relationship was not significant ($P > 0.05$) possibly due both to the low number of match-ups ($N = 11$) and two outlier values (Fig. 5 D).

3.4. Comparison of ESA OC-CCI and L8-OLI products

The aim of using ESA OC-CCI *Chla* V5 product was twofold. First, this allowed to compare remotely sensed data with field observations available prior to 2013. Second, this enabled to cross validate with L8-OLI outputs on the same bounding box than for ESA OC-CCI (Fig. 1) for the period 2013–2021. Remotely sensed *Chla* estimated by ESA OC-CCI product ranged between 0.11 and 0.91 µg L^{-1} with a mean ± sd of 0.31 ± 0.11 µg L^{-1} ($N = 1844$; Fig. 6A). A strong seasonal variability in *Chla* was detected with either one peak per year before 2012 or two peaks per year after 2012. The observations of extracted *Chla* from past studies matched well with the remotely sensed data (Fig. 6A). Unlike for survey sites 1 and 2 (Fig. 5 A, B), the dynamics of SST and *Chla* (Fig. 6A) were opposite and negatively correlated at the lagoon scale ($r = -0.29$, $t = -4.37$, df = 207, $P < 0.001$). Remotely sensed *Chla* values by L8-OLI followed the same trend than from ESA OC-CCI for the period 2013 to 2021 (Fig. 6B). The relationship between the two methods was linear and highly significant and the slope was close to 1 (Fig. 6C).

3.5. Modelling of life-history traits of the pearl oyster

The first step was to calibrate the half saturation coefficient X_k of the scaled functional response of the *Pinctada margaritifera* DEB model using shell length values over six months retrieved from Sangare et al. (2020) at S1 and S3. The best X_k value was 0.34 µg L^{-1} leading to a good fit with observed values (Fig. 7A). Then, three traits of the pearl oyster were estimated using two forcing variables of the DEB model *i.e.* the remotely sensed values of *Chla* at the three sites and the MODIS SST from a central lagoon pixel (Figs. 1 and 2).

In the model, SST controls the metabolic rates through the temperature correction function (TC) and the assimilation rate is dependent on *Chla via* the scaled functional response (f). Determining the range of values taken by TC and f allows measuring their separate effects on life-history traits. TC averaged 1.72 with a coefficient of variation (CV = sd/mean) of 6.7 %. Mean (and CV) of f values were 0.55 (19.2 %), 0.45

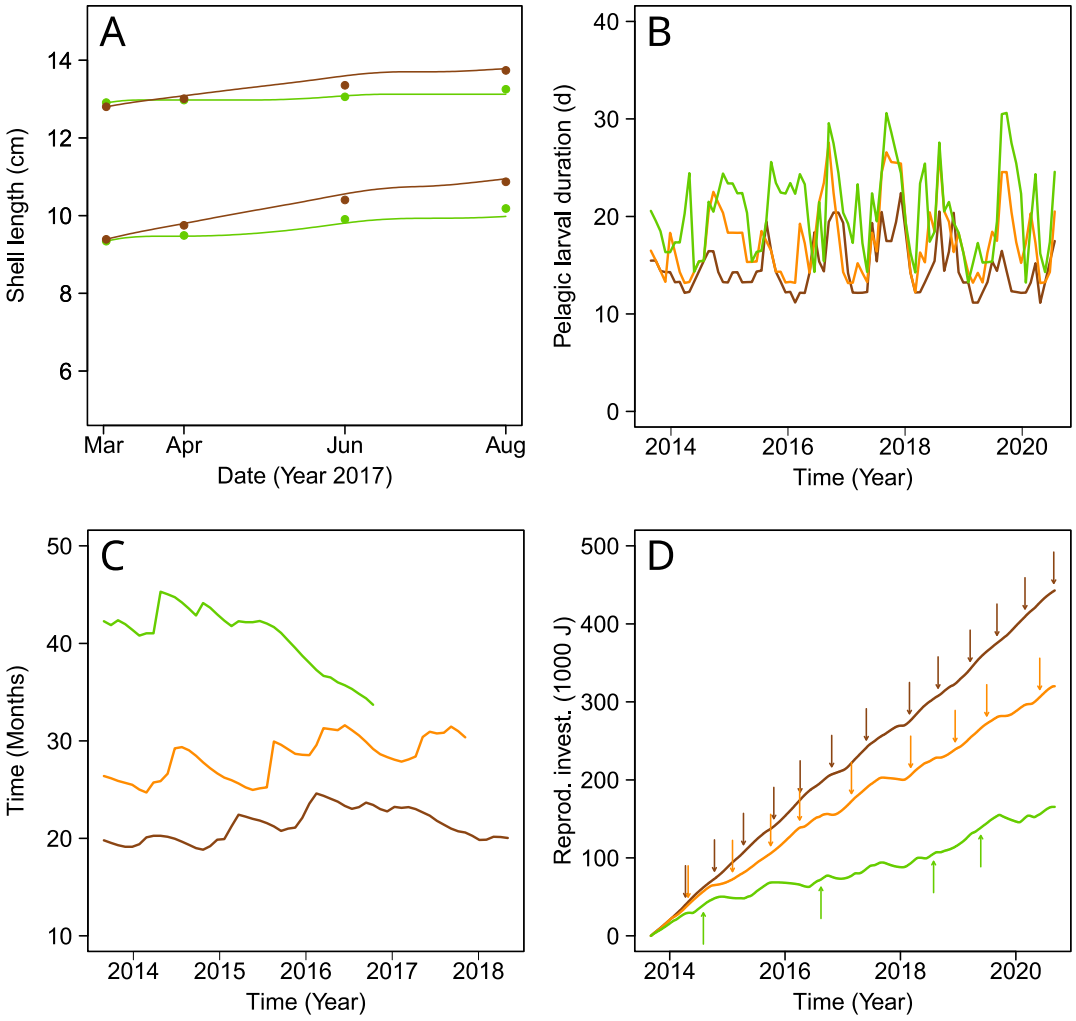

Fig. 7. DEB outputs for the three survey sites (S1 brown line, S2 orange, S3 green). A) DEB validation on Sangare et al. (2020) pearl oyster shell length values using a calibrated value of $X_k = 0.34$ µg L^{-1} in two sites (S1 and S3, filled circle are observations, lines are the simulations). B) Pelagic larval duration (PLD) estimated every month for the seven years. C) Time needed for a recently settled juvenile to reach grafting size (9 cm). D) Cumulative reproduction investment and potential spawning (arrows) of a 13 cm shell length adult. (For interpretation of the references to colour in this figure legend, the reader is referred to the web version of this article.)

(25.5 %) and 0.39 (30.7 %) for S1, S2 and S3 respectively. Therefore, f values in S3 were 29 % lower and 160 % more variable than in S1. Also, TC was less variable than f values.

Pelagic larval duration (PLD) displayed seasonal variations at the three sites but with different means and ranges (Fig. 7B). All survey sites combined, 50 % of the values ranged between 14.3 and 20.4 days. PLD in S1 showed the lowest values (from 11.1 to 22.4 days). PLD in S2 and S3 ranged higher than S1 (from 12.2 to 30.6 days). Differences between the sites were more pronounced for juvenile and adult traits which varied by approximately a factor two to three between S1 and S3 in particular (Fig. 7C). The mean times needed for recently settled juveniles to reach the grafting size (9 cm shell length) were 21.3, 28.3 and 40.6 months at S1, S2 and S3 respectively. The minimum value of this growth trait was 18.8 months in S1 and the maximum one was 45.3 months in S3. Temporal fluctuations of the different traits were mostly smoothed but still persisted. They were less the result of seasonality than of inter-annual differences in the forcing variables (SST and *Chla*). Each of the survey sites displayed a different temporal pattern over the seven and half years underlying spatio-temporal interactions in TC and f. Growth in S1 stayed rather stable, whereas it increased in S2, and decreased after a steady phase in S3. Cumulative reproduction investment displayed the same patterns. Reproductive investment of a 13 cm-shell length adult was regular as the cumulative output fit a straight line and spawning events occurred at periodic interval in S1 (Fig. 7D; 13 spawning events *i.e.* 1.7 year^{-1}). The same pattern occurred in S2 but with a lower food availability leading to 9 spawning events (1.2 year^{-1}) which were less regular. Some discrepancies were highlighted in S3 and characterized by a more variable reproductive investment which is reflected by irregular and less frequent spawning events (4 spawning events *i.e.* 0.5 year^{-1}).

4. Discussion

4.1. Relevance of remotely sensed products for a deep atoll lagoon

In the present study, two remotely sensed products were assessed to retrieve either sea surface temperature (SST) or chlorophyll *a* concentrations (*Chla*). First, MODIS-Aqua SST product performed well in reproducing the variations over a six-month period monitored in 2017 by Sangare et al. (2020). Using another SST product (the Multi scale ultra-high resolution; MUR), Van Wynsberge et al. (2020) showed that SST was well estimated in Raroia atoll, another deep atoll. Sensors with higher spatial resolution (*i.e.* 30 m aboard Landsat-8) would have provided higher spatial resolution but at the expense of a lower temporal frequency (minimal revisiting time of 16 days for L8). However, the weak spatial SST differences (0.3 °C) between S1 and S3 lead us to prefer a better temporal resolution especially as, in this range of uncertainty, life-history traits simulated by DEB models were little affected (Van Wynsberge et al., 2020).

Although Ahe atoll has concentrated most of the research programs for 15 years, the validation of satellite products used to retrieve *Chla* by historical *in situ* observations was not an easy task as the data are patchy and come from various sources using different quantification methods (Extracted *Chla*: Thomas et al., 2010, Lefebvre et al., 2012, Pagano et al., 2017; Rodier et al., 2021; *in vivo Chla* fluorescence recorded by *in situ* probes Sangare et al., 2020). This problem is inherent to remote coral reef and lagoon ecosystems and their higher investigation costs for continuous *in situ* monitoring.

Here, the validation of *Chla* retrieved with satellite products was satisfactory overall. A first temporal validation was carried out on two of the three survey sites using *in vivo* fluorescence data obtained by Sangare et al. (2020) from probes deployed over a 6-month period. Although the relationship was non-significant due to two outliers and the small amount of L8 images available for that period ($N = 11$), the amplitudes and trends of observed *Chla* were reproduced adequately. The discrepancies may also be explained by the probes themselves, as the fluorescence sensors are subject to biofouling but also to fluorescence quenching due to high light at day time (Monaco et al., 2021). In order to use older extracted *Chla* collected between 2007 and 2009 (from Thomas et al., 2010 and Lefebvre et al., 2012) before the launch of Landsat- 8, a comparison of the ESA OC-CCI and Landsat-8 OLI chlorophyll products was undertaken over the period 2013–2021. The two products gave similar values and trends, and this is a reassuring result given that they used different sensors, processing algorithms and atmospheric corrections. Also, the inter-annual and seasonal *Chla* trends observed *in situ* during the period 2007–2009 fitted well with the ESA OC-CCI product.

However, it is the spatial validation exercise that provides the most interesting validation of remote sensing methods. We remind that the closest scene available to retrieve remote sensed *Chla* of the spatial transect was one month later that the *in situ* sampling. Fortunately, *Chla* were low and quite stable at this period (end of autumn, Fig. 5), and therefore we assumed the two data sets were comparable. On the one hand, this exercise makes it possible to validate the product over a range of values (about 0.1 to 0.4 μg L^{-1}) comparable to the range of average temporal variations and, on the other hand, it allows to empirically determine the depth at which the bottom reflectance no longer has an impact on the data (depth up to 20 m). This agreed with the findings of Ackleson et al. (2018) who theoretically showed that the maximum depth at which benthic cover could be detected in coral reefs was 11.4, 18.4 and 21.6 m for benthic algae, coral, and uncolonized sand bottom types respectively.

Results from the present study allows to state that the combined used of L8-OLI sensor coupled to ACOLITE atmospheric correction and the OC3CI *Chla* algorithm are appropriate for the study of spatio-temporal variations of *Chla* in deep atoll lagoons and for depth higher than 30 m. Applicability to other deep atolls is high: some 13 atolls out of 26 studied in Pagès and Andréfouët (2001) shows a mean depth higher than 28 m. Another motivation to use high spatial resolution sensor similar to L8-OLI's, is the presence of coral pinnacles in atoll lagoons and the fact that all lagoons are not wide enough to be studied at a kilometric spatial resolution available with most other Ocean Colour products. The problem of pinnacles would be even more striking in many atoll lagoons compared to Ahe, such as Raroia, Takapoto or Manihiki, three other deep pearl farming atolls with numerous pinnacles (Andréfouët et al., 2020).

4.2. Insight in phytoplankton biomass temporal dynamics

For the first time, a long-term and homogeneous series of chlorophyll *a* concentrations at high spatial resolution (*Chla* a proxy of phytoplankton biomass) and water temperature is available for an atoll lagoon. These new data confirm spatial patterns identified during short expeditions, but more importantly, they highlight a seasonality that was not previously evidenced in Ahe atoll. The first spatial and temporal data set on *Chla* in Ahe atoll were collected by Thomas et al. (2010) over 4 periods of 15 to 30 days each between April 2007 and March 2008. At this observation scale, these authors showed that the day to day variability was higher than the seasonal one, and that this could be linked to the wind driven mixing effect of the water column. Lefebvre et al. (2012) showed in the same atoll a more pronounced seasonality of *Chla* in relation to temperature the following year (over the period May 2008–August 2009), but their sampling schemes were not adapted to discuss the day to day variability. The data retrieved thanks to the ESA OC-CCI products shed light on these trends as they show a marked difference between these two periods (2007/2008 and 2008/2009). Thomas et al. (2010) potentially missed a *Chla* peak in June 2007 and *Chla* variations were more pronounced the following year. While variations on small temporal scales were also evidenced by the ESA OC-CCI product (Fig. 5), which would require further specific studies, this series clearly shows intra- and inter-annual patterns.

Seasonal variations in phytoplankton biomass have already been

reported in similar atoll or coral reef ecosystems. Buestel and Pouvreau (2000) showed a weak seasonality of *Chla* in a closed atoll (Takapoto) in the period 1990–1991, while Charpy (1996) showed a more marked seasonality in the same atoll for the following year 1992. In a study on the island mass effect in coastal Rangiroa atoll waters (*i.e.* outside the lagoon), Vollbrecht et al. (2021) showed a seasonality of *Chla* and a positive relationship with temperature over the period 2003–2019. They interpreted this increase in biomass in the atoll coastal environment as the result of an advection of dissolved and particulate materials from the lagoon through the pass. Net exchanges of plankton from the lagoon to the open ocean had also been shown on Ahe atoll through the atoll rims (Pagano et al., 2017). Vollbrecht et al. (2021)'s result could be interpreted as an indirect proof of seasonality of *Chla* within the Rangiroa lagoon, although this could be also related to the seasonal wave regimes (Dutheil et al., 2020), which also controls export through the passes. Elsewhere, this seasonality of *Chla* has also been shown on open coral ecosystems in the Red Sea by satellite products with one or two biomass peaks per year (Racault et al., 2015).

The seasonality of *Chla* may have two main sources: seasonal variations in water temperature and availability of resources needed for phytoplankton growth and/or seasonal variations in water mass exchanges between the lagoon and the adjacent waters. In Ahe lagoon, phytoplankton is limited by the availability of dissolved nitrogen and primary production is supported mainly (*ca* 2/3) by regeneration processes of dissolved organic nitrogen endogenous to the atoll lagoon (Rodier et al., 2021). The results of the present study showed a relationship of *Chla* with water temperature in survey sites S1 and S2. It is most likely that higher temperature increases the nitrogen regeneration processes *via* grazing by zooplankton or the microbial loop, process which increases the resource availability for phytoplankton growth (Seceh et al., 2021). But, other sources of exogenous nitrogen are also part of the picture, such as atmospheric deposition through rainfall (Ren et al., 2017), atmospheric nitrogen fixation, or bird colonies among others (Rodier et al., 2021). A temporal variability in the inputs of these exogenous sources could also control the seasonal patterns in *Chla*. For example, the rainy season usually starts in November for 6 months and precedes the increase in phytoplankton biomass. On the other hand, Ahe is considered as semi-enclosed atoll with water exchanges through the pass and with water imports mainly through spillways (named *hoa*) driven by waves (Fig. 1; Andréfouët et al., 2022a). Studies by Andréfouët et al. (2001) and Chevalier et al. (2017) showed a significant and positive relationship between the residence time of water masses in lagoons (or the age of water masses) and *Chla* at the lagoon scale. Very recently, an extensive study of the influence of waves on the age of water masses in Ahe over a long period (between 2000 and 2018) indicates very clearly, a seasonality of water mass age at the annual scale but also significant inter-annual differences before and after the period 2011–2012 (Andréfouët et al., 2022a). This could partly explain the temporal dynamics of phytoplankton with a marked seasonality before 2012 followed after 2012 by two biomass peaks per year, which would deserve further study.

4.3. The role of the lagoon hydrodynamics

From a spatial point of view, the identified pattern, *i.e.* an increase in *Chla* towards the south-west of the lagoon (Fig. 4), was well-known and seems to be a permanent feature. Thomas et al. (2010) and Lefebvre et al. (2012) evidenced this pattern over the period 2007–2009 at different seasons and Rodier et al. (2021) identified it again some 10 years later (Nov.-Dec. 2017). The lagoon hydrodynamics is mainly dominated by a wind driven overturning circulation (Dumas et al., 2012). Under typical trade winds, two main barometric water circulations emerge: a dominant anticlockwise cell in the north occupying 2/3 of the lagoon, and a clockwise cell for the southern part. In addition, a central cell in front of the pass (west), is more or less present depending of the wind intensity and direction, and depends mostly on tidal flushing (Dumas et al., 2012). The e-flushing time, the time needed to decrease a concentration of a particle by a factor 2.178 (e^1), is typically higher in the south cell compared to the central area (80 days *versus* 50 days) possibly leading to higher phytoplankton biomass, a process also shown at the lagoon scale (Andréfouët et al., 2001). These hydrodynamic features and the higher cultured pearl oyster standing stocks and human density in the south (with possible anthropogenic-driven nutrient enrichment) were the most probable explanations of a higher *Chla* in this area (Lefebvre et al., 2012; Rodier et al., 2021). However, the present study offers new perspectives in the spatio-temporal patterns of the phytoplankton biomass. The three survey sites were located on purpose in different circulation zones and present different variability of e-flushing times depending on wind intensity and direction: S1 belongs the south circulation cell, S2 is at the confluence of the north and south cells and S3 is in the northern cell (Dumas et al., 2012). The survey of these sites showed that they did not follow the same temporal trends whereas Lefebvre et al. (2012) stated that there were no spatio-temporal interactions at the lagoon scale. Although seasonality was present in each of the survey sites, the correlation with temperature was weaker for S2 than for S1 and was insignificant for S3. A positive correlation between *Chla* and temperature at the lagoon scale had previously been shown (Thomas et al., 2012; Lefebvre et al., 2012) but our study reveals that it is clearly dependent on the studied sites. This may be a consequence of the lagoon's wind driven internal circulation and associated residence times (Dumas et al., 2012) in equilibrium with spatialized processes of phytoplankton growth (Rodier et al., 2021). Eventually, only 3D hydrodynamic modelling studies coupled with biogeochemical models will be able to decipher physical and biogeochemical processes in time and space (Seceh et al., 2021) and remotely sensed data would help to validate them.

4.4. Quantification of life-history traits of the black pearl oyster in natural conditions

The most complete and recent parameterisation of the DEB model for this species (Sangare et al., 2020) was used, with the exception of the half-saturation coefficient of the scaled functional response (X_k), which was re-adjusted to 0.34 $\mu g\,L^{-1}$ (rather than 0.2 $\mu g\,L^{-1}$ in Sangare et al., 2020) in order to fit the observed data. The value of X_k depends on the quality of the food, the food proxy used and its method of quantification and is classically free fitted when modelling one species in contrasting environments (Alunno-Bruscia et al., 2011). For example, Monaco et al. (2021) had to readjust this parameter X_k to a value of 0.36 $\mu g\,L^{-1}$ for black lip pearl oysters located in Takaroa Atoll and using *in vivo* fluorescence measurements. Thomas et al. (2011a) calibrated X_k at 0.3 $\mu g\,L^{-1}$ for larval stages of *Pinctada margaritifera* reared in *in situ* mesocosms at Ahe, but for a significantly different overall DEB parameterisation. It should be kept in mind that total *Chla* is assumed to be a correct proxy for the food available to pearl oysters, but far from ideal since only 20 % of this total phytoplankton biomass (nano-phytoplankton part) is really consumable by these organisms (Loret et al., 2000; Fournier et al., 2012a). It is therefore necessary to make the assumption of a constant ratio between picoplanktonic and nano-phytoplanktonic biomasses, which is not always valid at all spatial and temporal scales in Ahe lagoon (Lefebvre et al., 2012). These limitations may partly explain the differences between studies. In our case, it is rather due to differences in the quantification methods of *Chla* (remotely sensed *vs in vivo* fluorescence) as we use the same growth data as Sangare et al. (2020). However, our estimate of X_k is within the expected values from the literature.

Pearl oyster aquaculture takes place entirely in lagoons and is therefore highly dependent on natural environmental variability (food availability and water temperature) impacting larval capture, juvenile/adult growth (which will be grafted for pearl production), and adults reproduction (Andréfouët et al., 2022b). Thus, here, pelagic life duration (PLD), juvenile growth and adult reproduction were quantified

using spatial and temporal series of chlorophyll *a* concentrations (*Chla* used as a proxy of food availability) and sea surface temperature (SST) obtained from satellite products as forcing variables of a DEB model calibrated for this species (Sangare et al., 2020). This strategy should allow to obtain realistic values of these traits under natural conditions where temperature and food availability fluctuate more or less closely. It should be noted that the temperature correction (TC) of the metabolic rates in the model was less variable (CV = 6.7 %) than the scaled functional response (f) in the different sites (CV = 19 to 31 %). Food availability (*i.e. Chla*) then has a greater impact on life history trait values more than SST if we consider the effects of these forcing variables separately. However, since SST and *Chla* co-varied positively in S1 and S2 but not in S3, the cumulative effect of TC and f increased the difference in life-history trait values between the sites.

Pelagic larval duration (PLDs) is a critical life-history trait for understanding the time an individual spends in the water column and thus the potential for its spatial dispersal before settlement on a benthic substrate (Thomas et al., 2016). Sangare et al. (2019) observed PLDs between 18 and 31 days in experiments where food availability was fixed at different levels and for a mean temperature of 28.1 °C. A quantification of this PLD by simulation based on representative values of *Chla* and temperature throughout the Tuamotu-Gambier spatial range reached between 10 and 50 days (Sangare et al., 2020). However, these authors underline the strong interest of obtaining realistic spatio-temporal data of *Chla* and temperature to confirm the local life-history traits of the oyster. In our study, we showed that the main driver of PLD values was temporal variability rather than spatial variability between the three studied sites. Our PLD estimates thus varied from 11 to 30 days, *i.e.* in the low range of the estimates provided by Sangare et al. (2020). It should be noted that our quantification of PLD trait is in an Eulerian mode (for a given site), whereas in reality the larvae are subject to hydrodynamics and disperse spatially, and thus can possibly encounter different conditions. Our estimates are therefore to be used as a range of possible values over time but not at given sites. In an approach coupling a 3D hydrodynamic model and a DEB model, Thomas et al. (2016) showed that the PLD lasted from 12 to >28 days for the years 2007 and 2008. These authors also showed that the temporal variability of potential spat collection was much greater than the spatial variability. Our results are consistent with these data.

Spatial variability is much more pronounced for the other two life-history traits, namely the time to reach the commercial size and reproductive investment, while the temporal component is smoothed and representative of inter-annual variations due to the integrative physiological responses of the organisms. However, spatial and temporal components sometimes interact as these traits showed the greatest variability over time in S3 where SST and *Chla* did not correlate. In a study based on theoretical simulations crossing constant values of temperature and food availability, Sangare et al. (2020) obtained values between 15 and 40 months to reach commercial sizes at 9 cm, which more or less corresponds to the range of values we modelled over time. However, these authors point out that the fluctuations in the forcing variables have the greatest impact on the modelled traits. By oscillating either temperature or food availability, they obtained values between 25 and 27 months to reach commercial size and 2 to 5 spawning events per year for 13 cm shell length adults. We predict 0.5 to 1.7 spawning events per year under natural conditions. Few *in situ* data are available for comparison. Pouvreau and Prasil (2001) estimated from *in situ* growth data in several atolls and Von Bertalanffy-type models that 21 to 26 months were required to produce 10 cm shell length pearl oysters. Going from 9 cm to 10 cm requires an average of 3.1, 4.6, and 7 additional months for survey sites S1, S2 and S3 respectively in our simulations. While growth in sites S1 and S2 are in the high (19.8 + 3.1 = 22.9 months) and low (25.6 + 4.6 = 30.2) ranges respectively of the data collected by Pouvreau and Prasil (2001), growth in site S3 was particularly low (35.1 + 7 = 42.1 months). Therefore, the choice of sites has a very strong impact on oyster growth, but this is also true for the investment in reproduction, which can vary by as much as twofold between our environmentally contrasted sites. Our results show strong spatial and temporal effects for this trait in connection with the spatio-temporal variability of *Chla* since spawning events are closely synchronized with food availability (Fournier et al., 2012b). Thomas et al. (2012) showed that the spat collection of pearl oysters could be lower and more time-varying at a site located in the north water circulation cell (according to Dumas et al., 2012 see above), whereas it was stronger and less variable at a site located in the southern cell. Similarly, these authors show a higher abundance of bivalve larvae (including but not limited to *Pinctada margaritifera*) in the water column during warmer periods (February–May) when phytoplankton biomasses are usually higher and adult reproduction is stronger. The larvae count results of Thomas et al. (2012) represent the cumulative effect of spawning and PLD and indirectly support the spatial and temporal patterns we found.

5. Conclusion

Our study shows the feasibility of using satellite high spatial resolution sensors to produce realistic chlorophyll *a* concentrations (*Chla*) series in atoll lagoons deeper than 30 m. These data while subject to their own limitations and biases, provide useful new insights to the long-term functioning of these remote and economically critical ecosystems. Spatial and temporal variabilities are evidenced and significant, with a seasonal signal in particular, which had been poorly characterized by short field campaigns so far. The coupling between satellite data and DEB modelling has also been successful in quantifying the value of pearl oyster life-history traits under natural conditions and in highlighting spatio-temporal patterns. Immediate applications of these outputs would be to enhance the identification of high production areas for juvenile/adult oysters and better model larval dispersal (Thomas et al., 2016). These will definitely help the spatial management of pearl farming activities at the lagoon level although the method is currently limited to farming areas at depths higher than 30 m. To overcome this limitation, it would be necessary to map the reflectance of the benthic cover, and then to remove the contribution of this bottom reflectance to the total signal. In itself, this is not a trivial task.

Several methodological perspectives are also emerging to further develop this work. More detailed studies of the analysis of temporal and spatial variabilities of chlorophyll in relation to climatic conditions (temperature, wind) and hydrodynamic forcing should be undertaken. From a technical remote sensing point of view, the coupling between different satellite products with high spatial resolution (L8-OLI) and high temporal resolution (ESA OC-CCI) will have to be strengthened, keeping in mind that some other products (*e.g.* Sentinel-3A/B-OLCI, 300 m/pixel with a revisit time of ~2 days) could be incorporated in the process (Pahlevan et al., 2022). An interesting prospect would be to produce spatio-temporal patterns of phytoplankton groups using the Physat method (Alvain et al., 2005; Navarro et al., 2017) in order to better understand the functioning of these ecosystems but also to better quantify the resource available for pearl oysters. Finally, these data should be very useful for validating time-series outputs of 3D biogeochemical model currently under development (Seceh et al., 2021).

CRediT authorship contribution statement

Sébastien Lefebvre: Conceptualization, Methodology, Software, Formal analysis, Investigation, Data curation, Writing – original draft, Visualization, Project administration, Funding acquisition. **Charles Verpoorter:** Conceptualization, Methodology, Software, Data curation, Writing – original draft. **Martine Rodier:** Investigation, Resources, Writing – review & editing. **Nathanaël Sangare:** Software, Investigation, Resources. **Serge Andréfouët:** Conceptualization, Writing – review & editing, Project administration, Funding acquisition.

Declaration of competing interest

The authors declare that they have no known competing financial interests or personal relationships that could have appeared to influence the work reported in this paper.

Data availability

Data will be made available on request.

Acknowledgments

This study was supported by the project Management of Atolls (MANA) funded by the Agence Nationale de la Recherche (ANR-16-CE32-0004). We would like to thank the CALCULCO team for their help and assistance. Some of the image computations were performed on resources provided by the SCOSI/ULCO (Service Commun du Système d'Information de l'Université du Littoral Côte d'Opale) Infrastructure for Computing through CALCULCO platform under the MANA project. The authors would like to thank USGS for the distribution of Landsat-8 Level-1 data, the NASA group for sharing the global Ocean Colour data, and Vanhellemont and K. Ruddick for the development and support of the ACOLITE software. This work is a contribution to the Ocean Colour Climate Change Initiative of the European Space Agency (http://www.esa-oceancolour-cci.org). The authors acknowledge two anonymous reviewers for their valuable comments and suggestions, and Augustin and Judy Mata for their hospitality in Ahe atoll. This paper is dedicated to our colleague and friend, Nathanaël Sangare, who passed away too soon.

References

Ackleson, S.G., Moses, W.J., Montes, M.J., 2018. Remote sensing of coral reefs: uncertainty in the detection of benthic cover, depth, and water constituents imposed by sensor noise. Appl. Sci. 8, 2691. https://doi.org/10.3390/app8122691.

Alunno-Bruscia, M., Bourlès, Y., Maurer, D., Robert, S., Mazurié, J., Gangnery, A., Goulletquer, P., Pouvreau, S., 2011. A single bio-energetics growth and reproduction model for the oyster *Crassostrea gigas* in six Atlantic ecosystems. J. Sea Res. 66, 340–348. https://doi.org/10.1016/j.seares.2011.07.008.

Alvain, S., Moulin, C., Dandonneau, Y., Breon, F.M., 2005. Remote sensing of phytoplankton groups in case 1 waters from global SeaWiFS imagery. Deep-Sea Res. I Oceanogr. Res. Pap. 52, 1989–2004. https://doi.org/10.1016/j.dsr.2005.06.015.

Andréfouët, S., Pagès, J., Tartinville, B., 2001. Water renewal time for classification of atoll lagoons in the tuamotu archipelago (French Polynesia). Coral Reefs 20, 399–408. https://doi.org/10.1007/s00338-001-0190-9.

Andréfouët, S., Ardhuin, F., Queffeulou, P., Le Gendre, R., 2012a. Island shadow effects and the wave climate of the Western tuamotu archipelago (French Polynesia) inferred from altimetry and numerical model data. Mar. Pollut. Bull. 65, 415–424. https://doi.org/10.1016/j.marpolbul.2012.05.042.

Andréfouët, S., Charpy, L., Lo-Yat, A., Lo, C., 2012b. Recent research for pearl oyster aquaculture management in French Polynesia. Mar. Pollut. Bull. 65, 407–414. https://doi.org/10.1016/j.marpolbul.2012.06.021.

Andréfouët, S., Genthon, P., Pelletier, B., Le Gendre, R., Friot, C., Smith, R., Liao, V., 2020. The lagoon geomorphology of pearl farming atolls in the Central Pacific Ocean revisited using detailed bathymetry data. Mar. Pollut. Bull. 160, 111580. https://doi.org/10.1016/j.marpolbul.2020.111580.

Andréfouët, S., Desclaux, T., Buttin, J., Jullien, S., Aucan, J., Le Gendre, R., Liao, V., 2022a. Periodicity of wave-driven flows and lagoon water renewal for 74 Central Pacific Ocean atolls. Mar. Pollut. Bull. 179, 113748. https://doi.org/10.1016/j.marpolbul.2022.113748.

Andréfouët, S., Lo-Yat, A., Lefebvre, S., Bionaz, O., Liao, V., 2022b. The MANA (MANagement of atolls, 2017–2022) project for pearl oyster aquaculture management in the Central Pacific Ocean using modelling approaches: overview of first results. Mar. Pollut. Bull. 178, 113649. https://doi.org/10.1016/j.marpolbul.2022.113649.

Boss, E., Zaneveld, J.R.V., 2003. The effect of bottom substrate on inherent optical properties: evidence of biogeochemical processes. Limnol. Oceanogr. 48, 346–354. https://doi.org/10.4319/lo.2003.48.1_part_2.0346.

Brigolin, D., Porporato, E.M.D., Prioli, G., Pastres, R., 2017. Making space for shellfish farming along the adriatic coast. ICES J. Mar. Sci. 74, 1540–1551. https://doi.org/10.1093/icesjms/fsx018.

Buestel, D., Pouvreau, S., 2000. Particulate matter in takapoto lagoon waters: potential food for cultivated pearl oysters. Oceanol. Acta 23, 193–210. https://doi.org/10.1016/s0399-1784(00)00111-0.

Charpy, L., 1996. Phytoplankton biomass and production in two tuamotu atoll lagoons (French Polynesia). Mar. Ecol. Prog. Ser. 145, 133–142. https://doi.org/10.3354/meps145133.

Chevalier, C., Devenon, J.L., Pagano, M., Rougier, G., Blanchot, J., Arfi, R., 2017. The atypical hydrodynamics of the Mayotte lagoon (Indian Ocean): effects on water age and potential impact on plankton productivity. Estuar. Coast. Shelf Sci. 196, 182–197. https://doi.org/10.1016/j.ecss.2017.06.027.

Delesalle, B., Sakka, A., Legendre, L., Pages, J., Charpy, L., Loret, P., 2001. The phytoplankton of takapoto atoll (Tuamotu archipelago, French Polynesia): time and space variability of biomass, primary production and composition over 24 years. Aquat. Living Resour. 14, 175–182. https://doi.org/10.1016/s0990-7440(00)01098-6.

Dufour, P., Harmelin-Vivien, M., 1997. A research program for a typology of atoll lagoons: strategy and first results. In: Lessios, H.A., MacIntyre, I.G. (Eds.), Proceeding of the 8th International Coral Symposium, Panama, pp. 843–848.

Dufour, P., Andréfouët, S., Charpy, L., Garcia, N., 2001. Atoll morphometry controls lagoon nutrient regime. Limnol. Oceanogr. 46, 456–461. https://doi.org/10.4319/lo.2001.46.2.0456.

Dumas, F., Le Gendre, R., Thomas, Y., Andréfouët, S., 2012. Tidal flushing and wind driven circulation of ahe atoll lagoon (Tuamotu archipelago, French Polynesia) from in situ observations and numerical modelling. Mar. Pollut. Bull. 65, 425–440. https://doi.org/10.1016/j.marpolbul.2012.05.041.

Dutheil, C., Andréfouët, S., Jullien, S., Le Gendre, R., Aucan, J., Menkes, C., 2020. Characterization of south Central Pacific Ocean wind regimes in present and future climate for pearl farming application. Mar. Pollut. Bull. 160, 111584. https://doi.org/10.1016/j.marpolbul.2020.111584.

Fournier, J., Dupuy, C., Bouvy, M., Couraudon-Reale, M., Charpy, L., Pouvreau, S., Le Moullac, G., Le Pennec, M., Cochard, J.C., 2012a. Pearl oysters *Pinctada margaritifera* grazing on natural plankton in ahe atoll lagoon (Tuamotu archipelago, French Polynesia). Mar. Pollut. Bull. 65, 490–499. https://doi.org/10.1016/j.marpolbul.2012.03.026.

Fournier, J., Levesque, E., Pouvreau, S., Le Pennec, M., Le Moullac, G., 2012b. Influence of plankton concentration on gametogenesis and spawning of the black lip pearl oyster *Pinctada margaritifera* in ahe atoll lagoon (Tuamotu archipelago, French polynesia). Mar. Pollut. Bull. 65, 463–470. https://doi.org/10.1016/j.marpolbul.2012.03.027.

Gordon, H.R., 1978. Remote-sensing of optical-properties in continuously stratified waters. Appl. Opt. 17, 1893–1897. https://doi.org/10.1364/ao.17.001893.

Harmel, T., Chami, M., Tormos, T., Reynaud, N., Danis, P.A., 2018. Sunglint correction of the multi-spectral instrument (MSI)-SENTINEL-2 imagery over inland and sea waters from SWIR bands. Remote Sens. Environ. 204, 308–321. https://doi.org/10.1016/j.rse.2017.10.022.

Hu, C.M., Lee, Z., Franz, B., 2012. Chlorophyll a algorithms for oligotrophic oceans: a novel approach based on three-band reflectance difference. J. Geophys. Res. 117, C01011. https://doi.org/10.1029/2011jc007395.

Kerrigan, K., Ali, K.A., 2020. Application of landsat 8 OLI for monitoring the coastal waters of the US Virgin Islands. Int. J. Remote Sens. 41, 5743–5769. https://doi.org/10.1080/01431161.2020.1731770.

Kinsey, D.W., Hopley, D., 1991. The significance of coral reefs as global carbon sinks–response to greenhouse. Palaeogeogr. Palaeoclimatol. Palaeoecol. 89, 363–377. https://doi.org/10.1016/0921-8181(91)90117-F.

Kooijman, S.A.L.M., 2010. Dynamic Energy Budget Theory for Metabolic Organisation. Cambridge University Press, Cambridge, UK.

Kutser, T., Hedley, J., Giardino, C., Roelfsema, C., Brando, V.E., 2020. Remote sensing of shallow waters - a 50 year retrospective and future directions. Remote Sens. Environ. 240, 111619. https://doi.org/10.1016/j.rse.2019.111619.

Lefebvre, S., Claquin, P., Orvain, F., Veron, B., Charpy, L., 2012. Spatial and temporal dynamics of size-structured photosynthetic parameters (PAM) and primary production (^{13}C) of pico- and nano-phytoplankton in an atoll lagoon. Mar. Pollut. Bull. 65, 478–489. https://doi.org/10.1016/j.marpolbul.2012.04.011.

Loret, P., Le Gall, S., Dupuy, C., Blanchot, J., Pastoreaud, A., Delesalle, B., Caisey, X., Jonquières, G., 2000. Heterotrophic protists as a trophic link between picocyanobacteria and the pearl oyster *Pinctada margaritifera* in the takapoto lagoon (Tuamotu archipelago, French Polynesia). Aquat. Microb. Ecol. 22, 215–226. https://doi.org/10.3354/ame022215.

Maritorena, S., Morel, A., Gentili, B., 1994. Diffuse-reflectance of oceanic shallow waters - influence of water depth and bottom albedo. Limnol. Oceanogr. 39, 1689–1703. https://doi.org/10.4319/lo.1994.39.7.1689.

McCarthy, M.J., Colna, K.E., El-Mezayen, M.M., Laureano-Rosario, A.E., Mendez-Lazaro, P., Otis, D.B., Toro-Farmer, G., Vega-Rodriguez, M., Muller-Karger, F.E., 2017. Satellite remote sensing for coastal management: a review of successful applications. Environ. Manag. 60, 323–339. https://doi.org/10.1007/s00267-017-0880-x.

Monaco, C.J., Sangare, N., Le Moullac, G., Basset, C., Belliard, C., Mizuno, K., Smith, D.L., Lo-Yat, A., 2021. Dynamic energy budget model suggests feeding constraints and physiological stress in black-lip pearl oysters, 5 years post mass-mortality event. Mar. Pollut. Bull. 167, 112329. https://doi.org/10.1016/j.marpolbul.2021.112329.

Navarro, G., Almaraz, P., Caballero, I., Vazquez, A., Huertas, I.E., 2017. Reproduction of spatio-temporal patterns of major mediterranean phytoplankton groups from remote sensing OC-CCI data. Front. Mar. Sci. 4, 246. https://doi.org/10.3389/fmars.2017.00246.

O'Reilly, J.E., Maritorena, S., Mitchell, B.G., Siegel, D.A., Carder, K.L., Garver, S.A., Kahru, M., McClain, C., 1998. Ocean color chlorophyll algorithms for SeaWiFS. J. Geophys. Res. 103, 24937–24953. https://doi.org/10.1029/98jc02160.

Pagano, M., Rodier, M., Guillaumot, C., Thomas, Y., Henry, K., Andréfouët, S., 2017. Ocean-lagoon water and plankton exchanges in a semi-closed pearl farming atoll

lagoon (Ahe, tuamotu archipelago, French Polynesia). Estuar. Coast. Shelf Sci. 191, 60–73. https://doi.org/10.1016/j.ecss.2017.04.017.
Pagès, J., Andréfouët, S., 2001. A reconnaissance approach for hydrology of atoll lagoons. Coral Reefs 20, 409–414. https://doi.org/10.1007/s00338-001-0192-7.
Pagès, J., Andréfouët, S., Delesalle, B., Prasil, V., 2001. Hydrology and trophic state in takapoto atoll lagoon: comparison with other tuamotu lagoons. Aquat. Living Resour. 14, 183–193. https://doi.org/10.1016/s0990-7440(01)01113-5.
Pahlevan, N., Smith, B., Alikas, K., Anstee, J., Barbosa, C., Binding, C., Bresciani, M., Cremella, B., Giardino, C., Gurlin, D., Fernandez, V., Jamet, C., Kangro, K., Lehmann, M.K., Loisel, H., Matsushita, B., Ha, N., Olmanson, L., Potvin, G., Simis, S. G.H., VanderWoude, A., Vantrepotte, V., Ruiz-Verdù, A., 2022. Simultaneous retrieval of selected optical water quality indicators from Landsat-8, Sentinel-2, and Sentinel-3. Remote Sens. Environ. 270, 112860. https://doi.org/10.1016/j.rse.2021.112860.
Palmer, S.C.J., Gornez, P.M., Thomas, Y., Simis, S., Miller, P.I., Glize, P., Barillé, L., 2020. Remote sensing-driven Pacific oyster (*Crassostrea gigas*) growth modeling to inform offshore aquaculture site selection. Front. Mar. Sci. 6, 802. https://doi.org/10.3389/fmars.2019.00802.
Pouvreau, S., Prasil, V., 2001. Growth of the black-lip pearl oyster, Pinctada margaritifera, at nine culture sites of French Polynesia: synthesis of several sampling designs conducted between 1994 and 1999. Aquat. Living Resour. 14, 155–163. https://doi.org/10.1016/s0990-7440(01)01120-2.
Pouvreau, S., Jonquières, G., Buestel, D., 1999. Filtration by the pearl oyster, *Pinctada margaritifera*, under conditions of low seston load and small particle size in a tropical lagoon habitat. Aquaculture 176, 295–314. https://doi.org/10.1016/S0044-8486(99)00102-7.
Racault, M.F., Raitsos, D.E., Berumen, M.L., Brewin, R.J.W., Platt, T., Sathyendranath, S., Hoteit, I., 2015. Phytoplankton phenology indices in coral reef ecosystems: application to ocean-color observations in the Red Sea. Remote Sens. Environ. 160, 222–234. https://doi.org/10.1016/j.rse.2015.01.019.
Ren, H.J., Chen, Y.C., Wang, X.T., Wong, G.T.F., Cohen, A.L., DeCarlo, T.M., Weigand, M. A., Mii, H.S., Sigman, D.M., 2017. 21st-century rise in anthropogenic nitrogen deposition on a remote coral reef. Science 356, 749–752. https://doi.org/10.1126/science.aal3869.
Rodier, M., Pinazo, C., Seceh, C., Varillon, D., 2021. Pelagic stocks and carbon and nitrogen uptake in a pearl farming atoll (Ahe, French Polynesia). Mar. Pollut. Bull. 167, 112352. https://doi.org/10.1016/j.marpolbul.2021.112352.
Ruiz-Verdu, A., Jimenez, J.C., Lazzaro, X., Tenjo, C., Delegido, J., Pereira, M., Sobrino, J. A., Moreno, J., Ieee, 2016. Comparison of Modis and Landsat-8 retrievals of chlorophyll-a and water temperature over lake Titicaca. In: 36th IEEE International Geoscience and Remote Sensing Symposium (IGARSS), Beijing, PEOPLES R CHINA, pp. 7643–7646. https://doi.org/10.1109/igarss.2016.7730993.
Sangare, N., Lo-Yat, A., Le Moullac, G., Pecquerie, L., Thomas, Y., Beliaeff, B., Andréfouët, S., 2019. Estimation of physical and physiological performances of blacklip pearl oyster larvae in view of DEB modeling and recruitment assessment. J. Exp. Mar. Biol. Ecol. 512, 42–50. https://doi.org/10.1016/j.jembe.2018.12.008.
Sangare, N., Lo-Yat, A., Le Moullac, G., Pecquerie, L., Thomas, Y., Lefebvre, S., Le Gendre, R., Beliaeff, B., Andréfouët, S., 2020. Impact of environmental variability on *Pinctada margaritifera* life-history traits: a full life cycle deb modeling approach. Ecol. Model. 423, 109006. https://doi.org/10.1016/j.ecolmodel.2020.109006.
Seceh, C., Pinazo, C., Rodier, M., Lajaunie-Salla, K., Mazoyer, C., Grenz, C., Le Gendre, R., 2021. Biogeochemical model of nitrogen cycling in ahe (French Polynesia), a South Pacific coral atoll with pearl farming. Mar. Pollut. Bull. 169, 112526. https://doi.org/10.1016/j.marpolbul.2021.112526.
Sousa, T., Domingos, T., Kooijman, S.A., 2008. From empirical patterns to theory: a formal metabolic theory of life. Philos. Trans. R. Soc. Lond. Ser. B Biol. Sci. 363, 2453–2464. https://doi.org/10.1098/rstb.2007.2230.
Thomas, Y., Garen, P., Courties, C., Charpy, L., 2010. Spatial and temporal variability of the pico- and nanophytoplankton and bacterioplankton in a deep polynesian atoll lagoon. Aquat. Microb. Ecol. 59, 89–101. https://doi.org/10.3354/ame01384.
Thomas, Y., Garen, P., Pouvreau, S., 2011a. Application of a bioenergetic growth model to larvae of the pearl oyster Pinctada margaritifera L. J. Sea Res. 66, 331–339. https://doi.org/10.1016/j.seares.2011.04.005.
Thomas, Y., Mazurie, J., Alunno-Bruscia, M., Bacher, C., Bouget, J.F., Gohin, F., Pouvreau, S., Struski, C., 2011b. Modelling spatio-temporal variability of *Mytilus edulis* (L.) growth by forcing a dynamic energy budget model with satellite-derived environmental data. J. Sea Res. 66, 308–317. https://doi.org/10.1016/j.seares.2011.04.015.
Thomas, Y., Garen, P., Bennett, A., Le Pennec, M., Clavier, J., 2012. Multi-scale distribution and dynamics of bivalve larvae in a deep atoll lagoon (Ahe, French Polynesia). Mar. Pollut. Bull. 65, 453–462. https://doi.org/10.1016/j.marpolbul.2011.12.028.
Thomas, Y., Dumas, F., Andréfouët, S., 2016. Larval connectivity of pearl oyster through biophysical modelling; evidence of food limitation and broodstock effect. Estuar. Coast. Shelf Sci. 182, 283–293. https://doi.org/10.1016/j.ecss.2016.03.010.
Van Wynsberge, S., Le Gendre, R., Sangare, N., Aucan, J., Menkes, C., Liao, V.T., Andréfouët, S., 2020. Monitoring pearl farming lagoon temperature with global high resolution satellite-derived products: An evaluation using Raroia Atoll, French Polynesia. Mar. Pollut. Bull. 160, 111576. https://doi.org/10.1016/j.marpolbul.2020.111576.
Vanhellemont, Q., 2019. Adaptation of the dark spectrum fitting atmospheric correction for aquatic applications of the landsat and Sentinel-2 archives. Remote Sens. Environ. 225, 175–192. https://doi.org/10.1016/j.rse.2019.03.010.
Vanhellemont, Q., Ruddick, K., 2018. Atmospheric correction of metre-scale optical satellite data for inland and coastal water applications. Remote Sens. Environ. 216, 586–597. https://doi.org/10.1016/j.rse.2018.07.015.
Vollbrecht, C., Moehlenkamp, P., Gove, J.M., Neuheimer, A.B., McManus, M.A., 2021. Long-term presence of the island mass effect at Rangiroa atoll, French Polynesia. Front. Mar. Sci. 7, 595294. https://doi.org/10.3389/fmars.2020.595294.
Walton, C.C., Pichel, W.G., Sapper, J.F., May, D.A., 1998. The development and operational application of nonlinear algorithms for the measurement of sea surface temperatures with the NOAA polar-orbiting environmental satellites. J. Geophys. Res. Oceans 103, 27999–28012. https://doi.org/10.1029/98jc02370.
Wei, J.W., Lee, Z.P., Garcia, R., Zoffoli, L., Armstrong, R.A., Shang, Z.H., Sheldon, P., Chen, R.F., 2018. An assessment of Landsat-8 atmospheric correction schemes and remote sensing reflectance products in coral reefs and coastal turbid waters. Remote Sens. Environ. 215, 18–32. https://doi.org/10.1016/j.rse.2018.05.033.